Alexandria Engineering Journal (2016) 55, 663–671

HOSTED BY

Alexandria University

Alexandria Engineering Journal

www.elsevier.com/locate/aej
www.sciencedirect.com

ORIGINAL ARTICLE

Effect of cerium addition on corrosion behaviour of AZ61 + *X*Ce alloy under salt spray test

S. Manivannan [a,*], Sarathy Kannan Gopalakrishnan [a], S.P. Kumaresh Babu [a], Srinivasan Sundarrajan [b]

[a] *Department of Metallurgical and Materials Engineering, National Institute of Technology, Tiruchirappalli, Tamil Nadu 620 015, India*
[b] *National Institute of Technology, Tiruchirappalli, Tamil Nadu 620 015, India*

Received 5 January 2015; revised 1 October 2015; accepted 28 October 2015
Available online 19 November 2015

KEYWORDS

Magnesium;
Cerium;
Intermetallics;
Corrosion rate;
Ageing

Abstract The corrosion behaviour of Mg–6Al–1Zn + *X*Ce (where X = 0.5, 1.0, 1.5 and 2.0 wt% Ce) alloys, aged for 18 h at different temperatures of 180 °C, 200 °C, 220 °C and 240 °C, was studied in 3.5 wt% NaCl solution. The salt spray test was conducted in accordance with ASTM-B117 standard (fog test). The corrosion morphologies, corrosion rate and the composition of the corrosion products were investigated by X-ray Diffraction (XRD), Optical Microscopy (OM) and Scanning Electron Microscopy (SEM) techniques. The results show the cerium addition and ageing treatment has significantly influenced the corrosion morphologies and the corrosion rate. In AZ61 alloy, the intermetallic β ($Mg_{17}Al_{12}$) phase acts as a corrosion barrier and upon ageing the Al_4Ce phase precipitates along the α grain boundaries. The precipitation modifies the β phase to form more continuous network which subsequently reduces the corrosion attack in the chlorine environment. Salt spray test result shows the AZ61 alloy with 1.5 wt% Ce aged at 220 °C exhibits the better corrosion resistance.
© 2015 Faculty of Engineering, Alexandria University. Production and hosting by Elsevier B.V. This is an open access article under the CC BY-NC-ND license (http://creativecommons.org/licenses/by-nc-nd/4.0/).

1. Introduction

Recent decades have witnessed an increasing global demand for fast, light and efficient automobiles. This situation augmented by the increasing environmental and legislative influence, has further shifted the attention of automobile industries toward the usage of magnesium in auto parts [1]. Owing to its light weight, high specific strength to weight ratio, high damping capacity and recyclability, magnesium is more appealing than its counterparts, aluminium and steel [2,3]. The replacement by magnesium parts in automotive applications not only just provides weight savings but in fact has reduced vibration and overall noises on tuning. However, due to its active position in both EMF and sea water environment galvanic series, magnesium is always considered among the actively corroding metals. When pure magnesium is exposed to open atmosphere, its surface forms an oxide layer

* Corresponding author. Tel.: +91 9363301801.
E-mail addresses: manivannan.meta@gmail.com (S. Manivannan), sarathykannan11@gmail.com (S.K. Gopalakrishnan), babu@nitt.edu (S.P. Kumaresh Babu), sundar@nitt.edu (S. Sundarrajan).
Peer review under responsibility of Faculty of Engineering, Alexandria University.

http://dx.doi.org/10.1016/j.aej.2015.10.010
1110-0168 © 2015 Faculty of Engineering, Alexandria University. Production and hosting by Elsevier B.V.
This is an open access article under the CC BY-NC-ND license (http://creativecommons.org/licenses/by-nc-nd/4.0/).

which in the presence of moisture is converted to magnesium hydroxide. This hydroxide layer is stable at all basic pH ranges but unstable in acidic or neural range [4]. In basic pH ranges, passivation occurs as a result of formation of $Mg(OH)_2$. However, since the $Mg(OH)_2$ layer is water soluble, it does not provide a long term protection even in basic pH range [5]. In chloride, bromide, chlorate, sulfate and CO_2 acidified water environments the protective film breaks eventually rendering the metal surface active. Recent investigations on alloying AZ magnesium alloys with rare elements such as Ce, Y, Nd and Sr have witnessed an increase in creep and corrosion resistance. The addition of rare earth elements to these alloys suppresses the precipitation of deleterious β phase and instead, precipitates thermally stable phases such as Al_4RE and Al_2RE on the grain boundaries. Also, since the aluminum requirement for the formation of these stable phases is less, α grains are not left devoid of Al content. This eventually increases the corrosion resistance of the material [6–13]. Furthermore, magnesium is prone to scavenger effect i.e. presence of small impurities such as Fe, Ni, Cu and drastically reduces the corrosion resistance of the alloy, and the addition of rare earth elements in the magnesium alloy precludes the deleterious effect of those impurities by forming intermetallic compounds with them. They trap the impurities and decrease the activity of the cathode. Also, it is found that the surface oxide stability of the alloy is increased by the addition of rare earth elements [14]. The effect of cerium addition has been studied in detail by many researchers but the combined action of cerium addition followed by different ageing temperatures is still unexplored fully. In the present study, the effect of addition of cerium to AZ61 alloy and the effect of ageing temperature on the corrosion rate of the alloy subjected to NaCl environment have been extensively studied.

2. Experimental methods

Commercially pure Mg ingot (99.97 wt%), Al ingot (99.95 wt %), and Zn ingot (99.95 wt%) were melted in an electric resistance furnace with RJ2 protective flux to prepare AZ61 (Mg–6Al–1Zn, wt%) magnesium alloy. Mg–10 wt% Ce master alloy was added when the melt reached 720 °C and a 30 min reaction time was set for complete dissolution while stirring was done to attained homogeneity. The melt was poured into a mild steel cylindrical mould of dimensions 30 mm × 60 mm. For further analysis, samples were cut perpendicular to the axis of the prepared cast. The composition of the samples was determined by inductively coupled plasma atomic emission spectroscopy (ICP-AES) method and it is presented in Table 1. The as-cast samples were solution treated at a temperature of 450 °C for 16 h and then aged at different temperatures of 180 °C, 200 °C, 220 °C and 240 °C for 18 h. The salt spray experiment was carried out in ASCOTT S450*IS* salt spray chamber in accordance with ASTM B-117 standard. The test coupons were exposed in 3.5 wt% NaCl solutions up to 72 h and these coupons were intermittently evaluated at 24 h interval. After the test, the corrosion products were completely removed using chromate acid (180 g/l CrO_3 + 10 g/l $AgNO_3$) according to ASTM G1-03 standard practice for cleaning. The samples were then rinsed with acetone and dried in compressed air. The weight loss due to corrosion is determined and accordingly the corrosion rates were calculated. The microstructural observations of the samples were studied by using DIC Leica optical microscope. The X-ray Diffraction (XRD) technique confirmed the phases present in AZ61 + *X*Ce magnesium alloys. The presence of precipitates and corrosion morphologies were characterized using Hitachi Scanning Electron Microscope (SEM) and the elemental compositions in different phases were confirmed using Energy Dispersive Spectrometer (EDS).

3. Results and discussion

3.1. Microstructural observations

Fig. 1(a) shows the microstructure of as-cast AZ61 alloy. It consists of primary α grain with large β phase precipitated along the grain boundaries and some β phase precipitated within the α grains exhibiting a lamellar structure [15,16]. Fig. 1(b) shows the microstructure of solutionized AZ61 alloy which manifests the residuals of β phase, which are not completely dissolved into the matrix. Fig. 1(c) shows the microstructure of AZ61 alloy aged at 220 °C for 18 h. The microstructure comprises of α phase, β phase and β precipitates (fine dark particle) along the grain boundaries.

Fig. 2 shows the microstructures of the as-cast, solutionized (at 450 °C) and aged (at 220 °C) AZ61 + *X*Ce alloy (where x = 0.5, 1.0, 1.5 & 2.0 wt% of Ce). The addition of cerium to AZ61 alloy introduces a new Al–Ce phase, which refines the grain and retards the progression of β phase. The addition of cerium helps in increasing the corrosion resistance of the alloy in three ways: (i) by formation of rod like Al–Ce phases. This Al-rich Al–Ce phase forms even before the solidification of either of β and α phase, therefore reducing the amount of Al available for β formation and it acts as a nucleating agent for α-Mg, which leads to grain refinement [17]; (ii) by retarding the growth of those β phase, which causes galvanic corrosion by growing inside the grains; and (iii) by Song et al.'s dual role mechanism [18,19], i.e. causing fine distribution of remaining β phases along the grain boundaries, which helps in increasing the corrosion resistance by barrier effect. The β phases along the grain boundaries act as a corrosion barrier and increase the corrosion resistance of the AZ61 alloy. The effect of ageing treatment increases the amount of β phase. The β phase was formed in two different morphologies: (1) a large

Table 1 Chemical composition of the experimental alloys (in wt%).

Alloy	Al	Zn	Ce	Mn	Fe	Cu	Ni	Mg
AZ61 + 0.5Ce	5.546	1.008	0.5	0.33	0.012	0.004	0.0015	Bal.
AZ61 + 1.0Ce	5.504	1.009	1.0	0.33	0.012	0.004	0.0015	Bal.
AZ61 + 1.5Ce	5.582	0.9163	1.5	0.31	0.012	0.004	0.0015	Bal.
AZ61 + 2.0Ce	5.415	0.9604	2.0	0.32	0.012	0.004	0.0015	Bal.

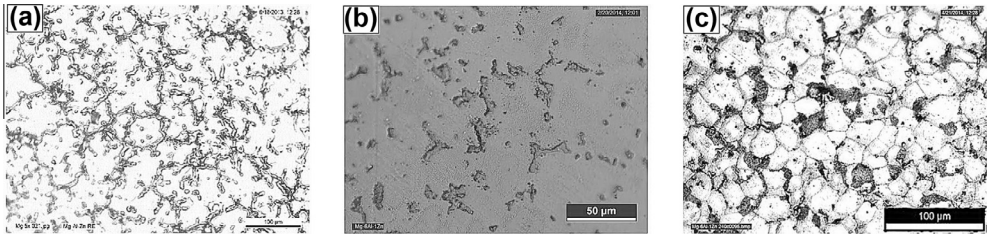

Figure 1 Microstructure of the as-cast AZ61 alloy. (a) As-cast, (b) solutionized at 450 °C and (c) aged at 220 °C.

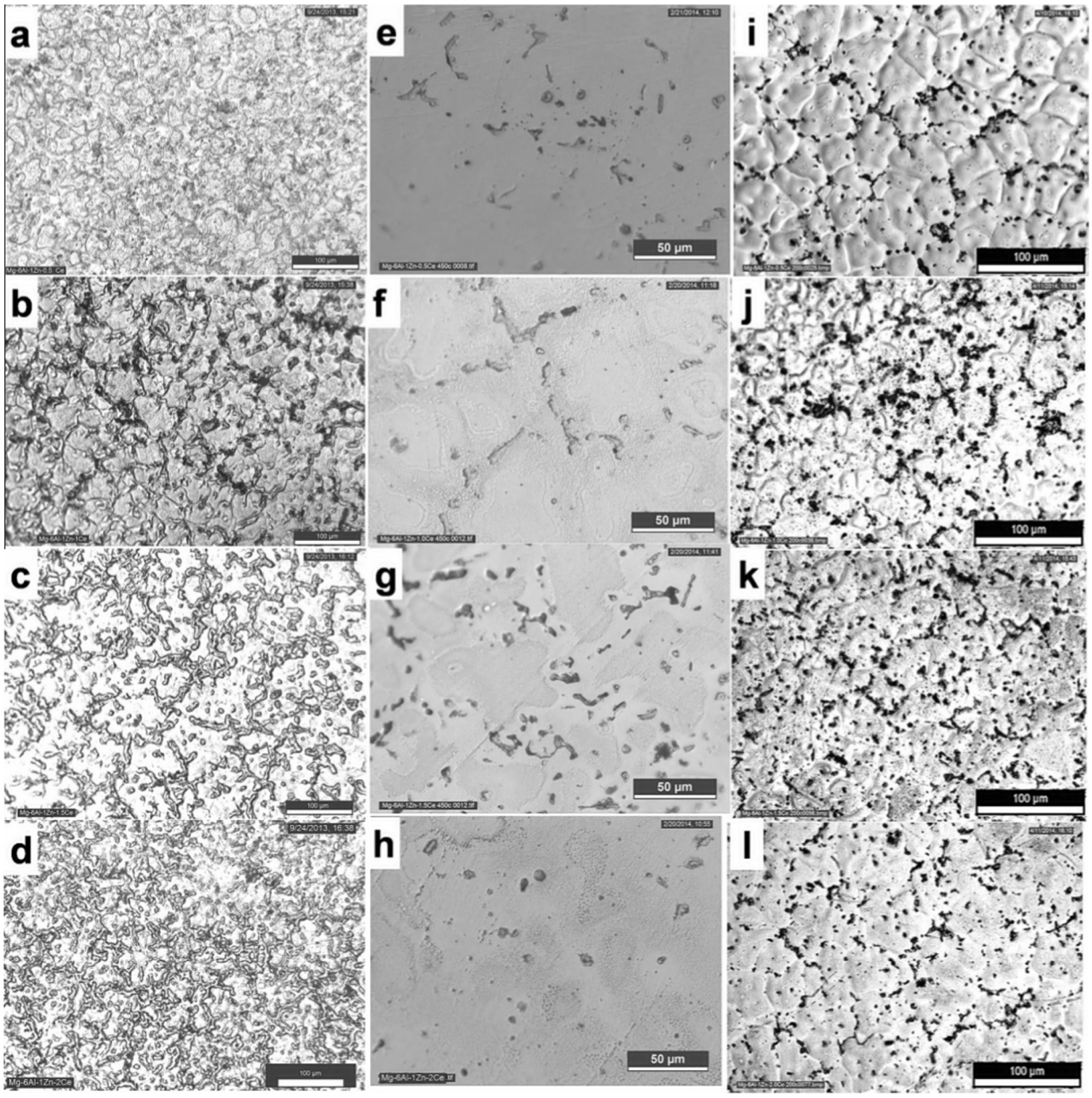

Figure 2 Microstructure of the as-cast AZ61 + *X*Ce alloy. $X =$ (a) 0.5, (b) 1.0, (c) 1.5 and (d) 2.0; solutionized at 450 °C for 16 h (e) 0.5, (f) 1.0, (g) 1.5 and (h) 2.0; aged at 220 °C for 18 h (i) 0.5, (j) 1.0, (k) 1.5 and (l) 2.0.

rod like continuous structure and (2) a discontinuous lamellar structure. Cerium addition has a little effect on the microstructure evolution of AZ61 on ageing. However, it retards the precipitation and growth of β phase. At lower ageing temperatures, the precipitation of β occurs rapidly in a continuous network along the grain boundaries. But on increasing the ageing temperature, the precipitation along the grain boundaries slows down and the β phase starts growing toward

the interior of the grain acquiring a lamellar structure. At initial temperatures of ageing, a continuous network of β acts as corrosion barrier and increases the corrosion resistance of the alloy. However on subsequent increase in ageing temperatures, the corrosion resistance begins to cease due to the decrease in the Al content in the interior of the grain due to the formation of β precipitates (Fig. 3).

3.2. Salt spray test

Fig. 4 illustrates the corroded surface morphology after salt spray test in 3.5 wt% NaCl solution. The macrostructures were observed after complete removal of corrosion products in AZ61 + *X*Ce alloys which were cleaned according to ASTM G1-03. In as-cast AZ61 alloy without Ce addition, the β phase forms micro-galvanic coupling and it accelerated the corrosion at α Mg matrix as shown in Fig. 4(a–d). It is evident that the extent and the depth of localized pitting attack are more in the base alloy and it is decreased subsequently with cerium additions. The corrosion process occurred in three stages: first being, initiation of small pits, followed by growth and spreading of deeper pits with an active front and finally the whole surface is more or less corroded with very large localized holes (diameter is up to mm) on the surface [17]. The base alloy has more or less attained the final stage after 72 h of exposure to 3.5 wt% NaCl solutions. However, in 0.5 and 1.0 wt% of Ce addition the corrosion is spread across the surface and attained second stage, whereas 1.5 and 2.0 wt% Ce addition exhibits only the first stage of pit growth. Fig. 5(a) and (b) illustrates overall corrosion rates varying with ageing temperature and cerium addition. It is concluded that the alloy with 1.5 and 2.0 wt% of cerium additions exhibits the good corrosion resistance at 220 °C ageing temperature. Fig. 6(a) illustrates the variation of corrosion rates with cerium addition at 240 °C and Fig. 6(b) shows the variation of corrosion rates with ageing temperature for 1.5 wt% Ce addition. It is found that the corrosion rate decreases with increasing cerium addition. This is due to the formation of Al–Ce phase along the α grain boundaries and retardation of growth of lamellar β phase inside the grain. With increase in ageing temperature, the corrosion rate first decreases, as the β phase acts as a corrosion barrier. However, after certain ageing temperature limit the corrosion rate increases due to the growth of lamellar β phase into the grains which decreases the aluminium content and causes galvanic corrosion.

3.3. X-ray diffraction

Fig. 7 shows X-ray diffraction patterns of (a) AZ61 aged at 220 °C, (b) AZ61 + 1.5 wt% Ce aged at 220 °C, (c) AZ61 + 2.0 wt% Ce aged at 220 °C and (d) AZ61 + 2.0 wt% Ce aged at 240 °C. The XRD pattern confirmed the presence of primary α, intermetallic β ($Mg_{17}Al_{12}$) phase and Al–Ce phase. The Al–Ce (Al_4Ce) phase identified and they are precipitated along the α grain boundaries. The intensity of Al–Ce peak increases with increasing cerium addition to the alloy.

3.4. SEM and EDS analysis

Fig. 8 shows the SEM image of AZ61 + 1.5 wt% Ce alloy aged at 220 °C. The SEM image indicates the different morphologies of β phase i.e. rod like β, round and lamellar β. The presence of intermetallic phases has been identified using EDS analysis which is further augmented by elemental

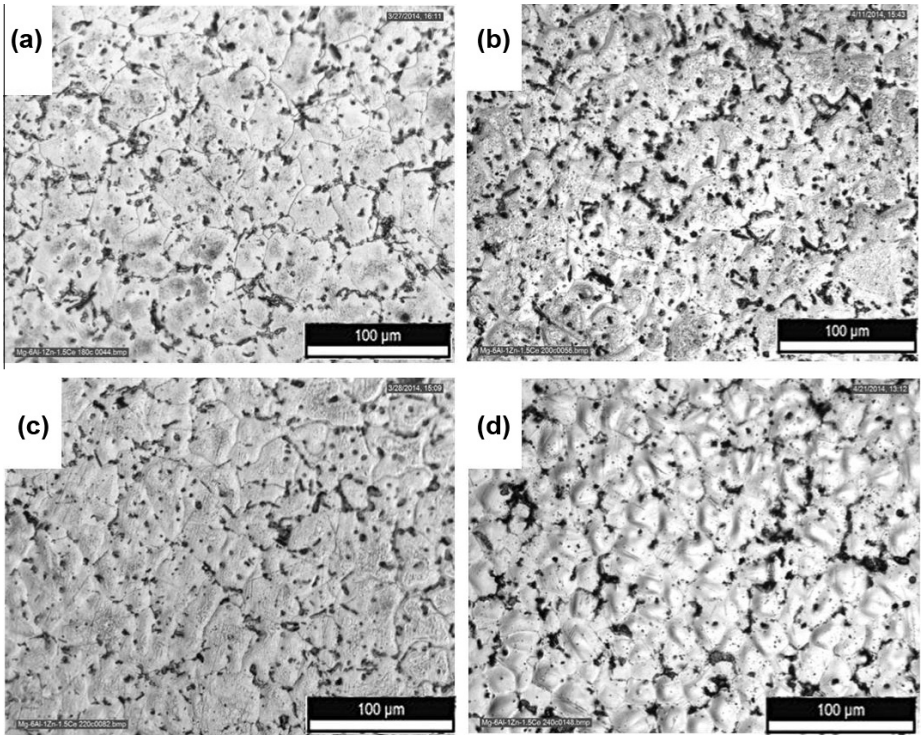

Figure 3 Microstructure of AZ61 + 1.5 wt% Ce aged at (a) 180 °C, (b) 200 °C, (c) 220 °C and (d) 240 °C.

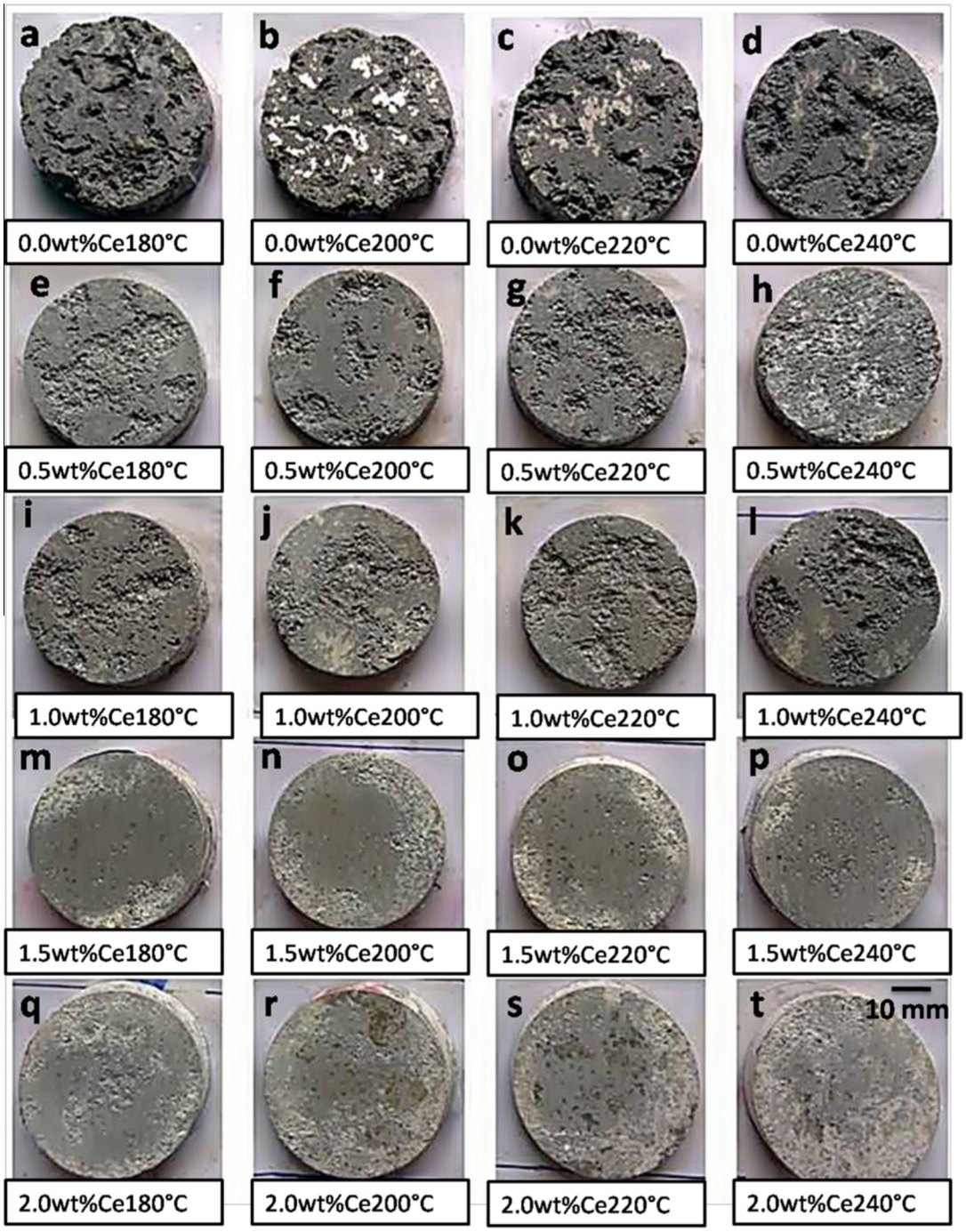

Figure 4 The surface morphology of AZ61 + *X*Ce alloy after 72 h of exposure in 3.5 wt% NaCl solution under salt spray test.

mapping. The presence of β and Al_4Ce phase marks a devoid of Mg content and clustering of Al content near the intermetallic phases in the elemental mapping. The eutectic magnesium near the intermetallic phase is rich in Al content than primary α phase. A galvanic cell is created due to the difference in solute concentration, with β acting as a cathode and thereby increasing the corrosion rate. But indeed an alloy with continuous and higher volume fraction of β phase inhibits corrosion by forming a stable passive film by barrier effect [20,21]. The elemental compositions of each phase are given in the EDS pattern. Fig. 9(a) and (b) shows the surface appearance of AZ61 + 1.5 wt% Ce aged at 200 °C and 220 °C respectively, exposed in 3.5 wt% NaCl salt spraying test for 72 h. The image has been captured after removal of corrosion products on the surface of the specimen. The sample surface was characterized by SEM and it confirms the presence of corrosion pits. The corrosion is affiliated with intermetallic phase, and the damage seen in Fig. 9 shows low corrosion attack in both ageing temperatures. The cracks were always initiated from any of these pits. Pitting corrosion is a localized type of corrosion which

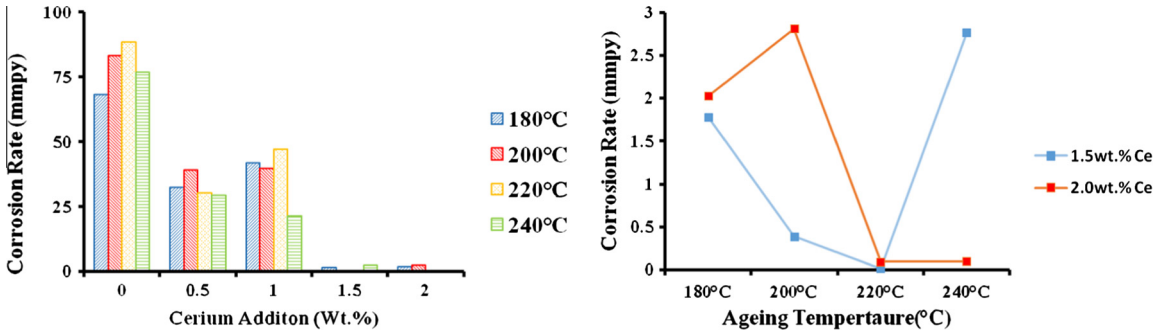

Figure 5 (a) Variation of corrosion rate in aged AZ61 + *X*Ce alloy and (b) corrosion rate vs. ageing temperature for 1.5 and 2.0 wt% Ce.

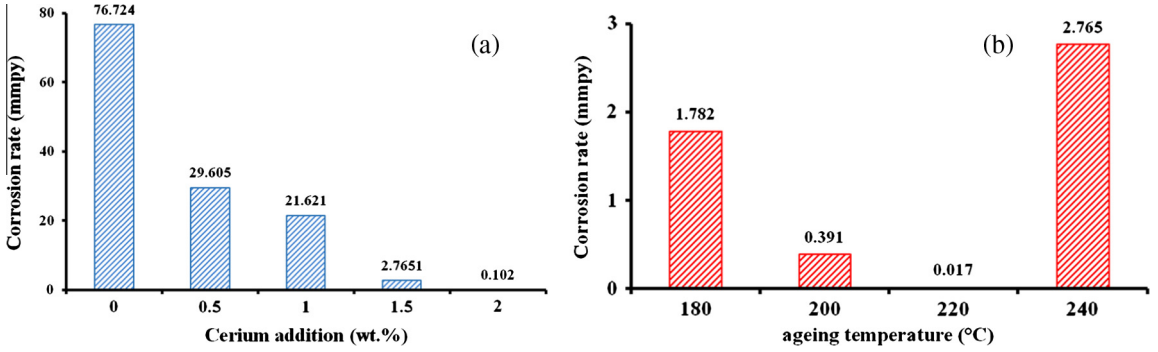

Figure 6 (a) Variation of corrosion rate with cerium addition at 240 °C ageing temperature and (b) variation of corrosion rate with ageing temperature at 1.5 wt% Ce addition.

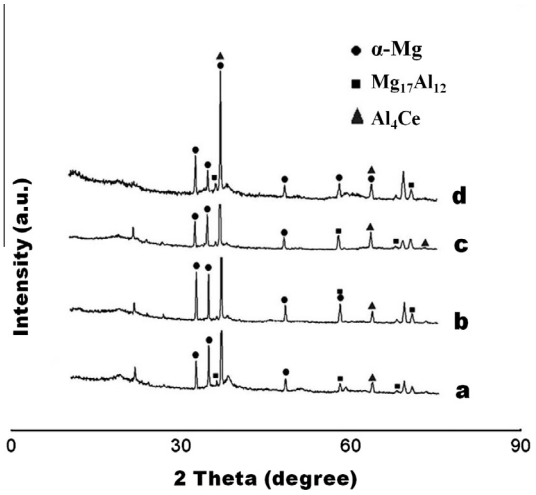

Figure 7 X-ray diffraction patterns of (a) AZ61 aged at 220 °C alloys, (b) AZ61 + 1.5 wt% Ce aged at 220 °C, (c) AZ61 + 2.0 wt % Ce aged at 220 °C, and (d) AZ61 + 2.0 wt% Ce aged at 240 °C.

occurs in the presence of aggressive chloride environment. The corrosion pit is easier to appear in α phase than in β phase. The α region surrounding the intermetallic β phase contains lesser Al than that of β due to solute depletion. Hence the α phase is easily corroded and the β phase flakes away because of the different corrosion potentials.

Fig. 10 is an example of the low corrosion attack in 3.5 wt % NaCl salt spray test. After exposed to 72 h of salt spraying, the alloy with 1.0 wt% Ce aged at 220 °C exhibits an oxide film on the surface that temporarily resists the local corrosion attack [5]. The SEM/EDS with elemental mapping techniques confirms the presence of intermetallic β ($Mg_{17}Al_{12}$) phase and Al_4Ce precipitates in the corroded surface. The presence of Al in the oxide layer that coats the AZ61 alloy in chlorine environment influences the surface activity. An improvement of corrosion resistance is attributed to segregation of Al on the surface.

4. Conclusion

1. On the addition of cerium to AZ61 alloy a new Al–Ce phase was formed. This new phase refines the α grain size and retards the growth of β phase. High degree of grain refinement is achieved at 1.5 wt% Ce addition.
2. With ageing temperatures, β phase grows rapidly in a continuous network. Hence, the corrosion resistance of the alloy is increased by barrier effect. However, above a certain limit, the continuous network growth along the grain boundaries ceases and the growth of β phase toward the interior of the grain accelerates. In 1.5 wt% Ce addition, the β grows in a continuous network up to 220 °C but above that temperature it starts growing toward the interior

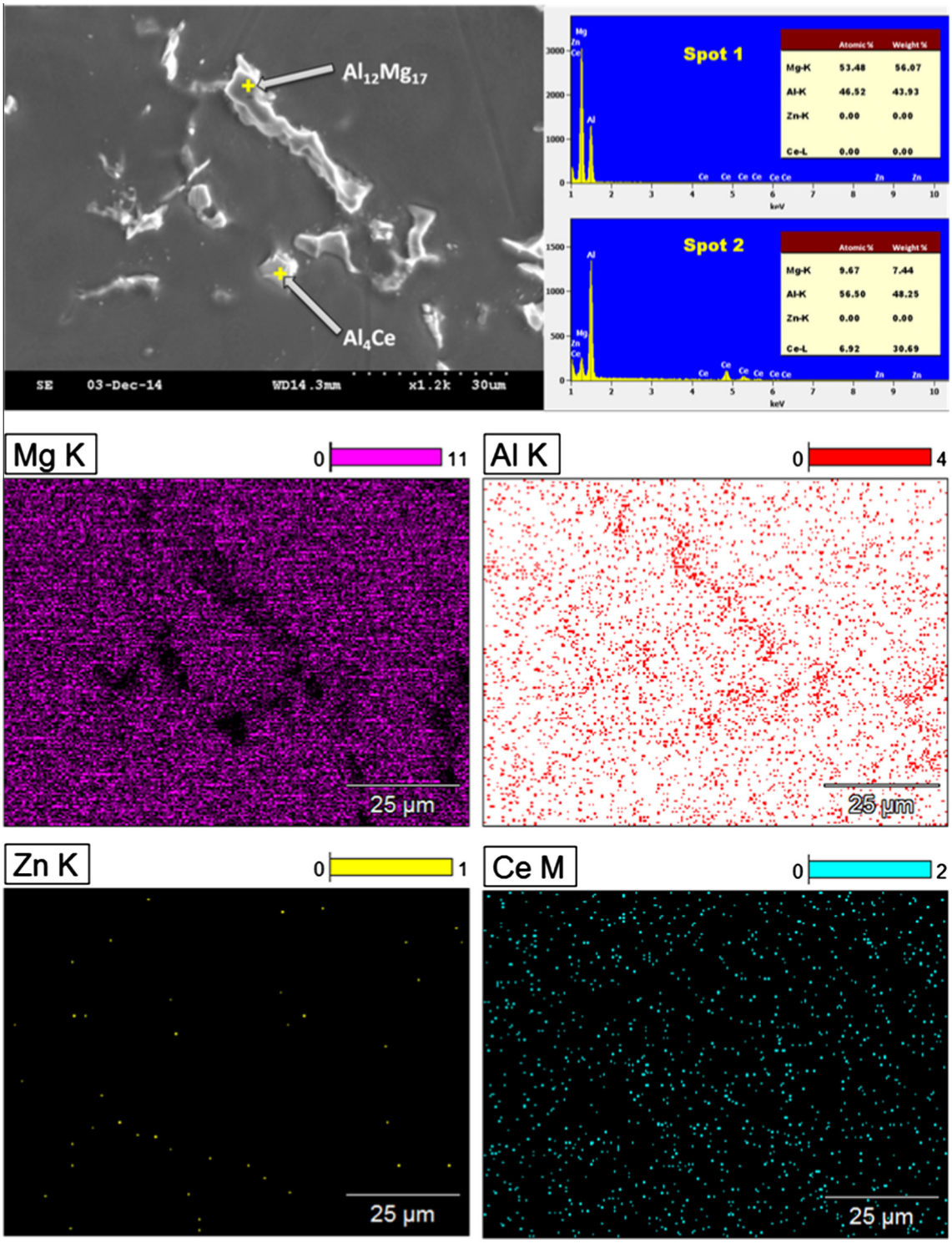

Figure 8 The SEM with EDS and elemental mapping of AZ61 + 1.5 wt% Ce aged at 220 °C after exposed in 3.5 wt% NaCl solution for 72 h.

of the grains. Since the galvanic corrosion is more pronounced than barrier effect when the continuous network of β phase is disintegrated, the corrosion resistance of the alloy begins to decrease.

3. In the salt spray experiment, alloys aged at 220 °C showed better corrosion resistance than other combinations. It showed only initial stages of pit growth after being exposed in 3.5 wt% NaCl salt spraying for 72 h.

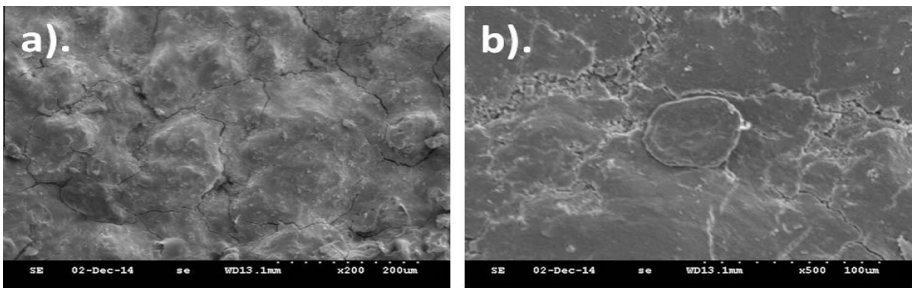

Figure 9 SEM morphologies after removing corrosion products on specimen surfaces of AZ61 + 1.5 wt% Ce alloy exposed in 3.5 wt% NaCl salt spraying test for 72 h (a) aged at 200 °C for 18 h and (b) aged at 220 °C for hours.

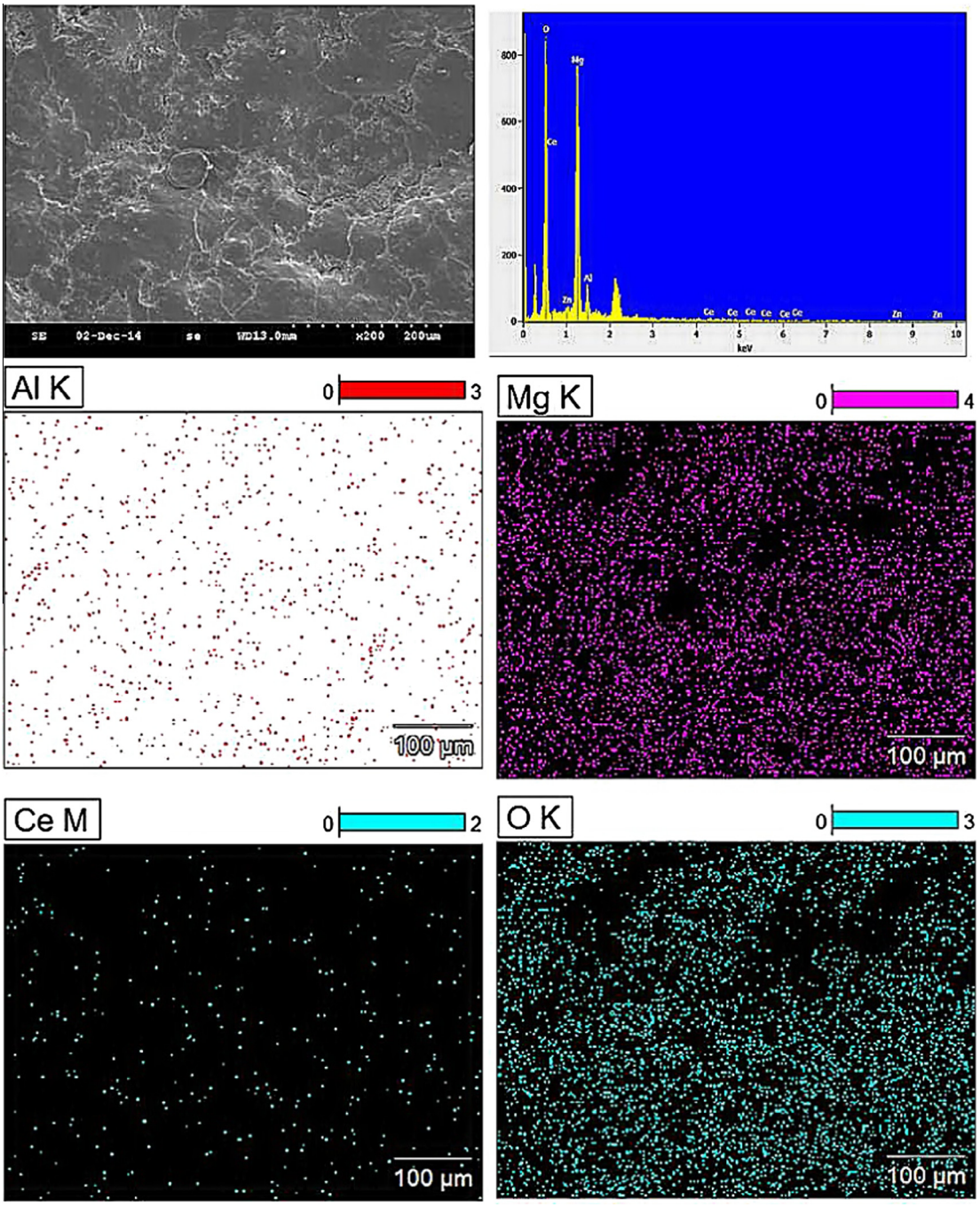

Figure 10 SEM/EDS and X-ray mapping of AZ61 + 1.5 wt% Ce aged at 220 °C after 72 h of exposure in 3.5 wt% NaCl solution.

Acknowledgements

This research work was supported by the Department of Metallurgical and Materials Engineering, NITT, India. The author is grateful for the support of TEQIP, NITT, India, for funding and facility provided throughout the research work. The authors wish to thank Dr. S. Sundarrajan, director of NITT and Dr. S.P. Kumaresh Babu, Associate Professor, Department of MME, NITT for their valuable supports in the experiments.

References

[1] E. Aghion, B. Bronfin, D. Eliezer, The role of the magnesium industry in protecting the environment, Mater. Process. Technol. 117 (2001) 381–385.
[2] B.L. Mordike, T. Ebert, Magnesium: properties—applications—potential, Mater. Sci. Eng. A 302 (2001) 37–45.
[3] K. Sugimoto, K. Niiya, T. Okamoto, K. Kishitake, A study of damping capacity in magnesium alloys, Trans JIM (1977) 277–288.
[4] Revised by Barbara A. Shaw, Pennsylvania State University. Corrosion Resistance of Magnesium Alloys. ASM Handbook, Volume 13A Corrosion: Fundamentals, Testing, and Protection, pp. 692–696.
[5] H.P. Godard, W.P. Jepson, M.R. Bothwell, R.L. Lane (Eds.), The Corrosion of Light Metals, John Wiley & Sons, 1967, pp. 283.
[6] Shou-Ren Wang, Microstructure and mechanical properties of AZ91 alloys by addition of yttrium, Mater. Eng. Perform. 18 (2009) 137–144.
[7] A. Sanschagrin, R. Tremblay, R. Angers, D. Dube, Mechanical properties and microstructure of new magnesium-lithium base alloys, Mater. Sci. Eng. A 220 (1996) 69.
[8] I.J. Polmear, Magnesium alloys and applications, Mater. Sci. Technol. 10 (1994) 1–16.
[9] I.J. Polmear, Recent developments in light alloys, Mater. Trans. JIM 37 (1996) 12.
[10] Yizhen Lu, Qudong Wang, Xiaoqin Zeng, Wenjiang Ding, Chunquan Zhai, Yanping Zhu, Effects of rare earths on the microstructure, properties and fracture behavior of Mg–Al alloys, Mater. Sci. Eng. 278 (2000) 66–76.
[11] Wenjuan Liu, Fahe Cao, Linrong Chang, Zhao Zhang, Jianqing Zhang, Effect of rare earth element Ce and La on corrosion behavior of AM60 magnesium alloy, Mater. Eng. 51 (2009) 1334–1343.
[12] D.H. Xiao, J.N. Wang, D.Y. Ding, H.L. Yang, Effect of rare earth Ce addition on the microstructure and mechanical properties of an Al–Cu–Mg–Ag alloy, Mater. Eng. 352 (2003) 84–88.
[13] Jinghuai Zhanga, Jun Wanga, Xin Qiu, Deping Zhang, Zheng Tian, Xiaodong Niu, Ding Xiang Tang, Jian Meng, Effect of Nd on the microstructure, mechanical properties and corrosion behavior of die-cast Mg–4Al-based alloy, J. Alloy. Compd. 464 (2008) 556–564.
[14] D. Hanawalt, C.E. Nelson, J. Peloubet, Corrosion studies of magnesium and its alloys, Trans. AIME 147 (1942) 273–281.
[15] C.H. Caceres, C.J. Davidson, J.R. Griffiths, C.L. Newton, Effects of solidification rate and ageing on the microstructure and mechanical properties of AZ91 alloy, Mater. Sci. Eng. A 325 (2002) 344–355.
[16] D. Duly, J.P. Simon, Y. Brechet, On the competition between continuous and discontinuous precipitations in binary Mg–Al alloys, Acta Mater. 43 (1995) 101–106.
[17] Faruk Mert, Carsten Blawert, Karl Ulrich Kainer, Norbert Hort, Influence of cerium additions on the corrosion behaviour of high pressure die cast AM50 alloy, Corros. Sci. 65 (2012) 145–151.
[18] G. Song, A. Atrens, Corrosion of Magnesium Alloys, Invited Refereed Review Article for Corrosion and Environmental Degradation of Materials, vol. 19, Wiley, New York, Mater. Sci. Technol., 2000.
[19] G. Song, A. Atrens, X. Wu, B. Zhang, Corrosion behaviour of AZ21, AZ501 and AZ91 in sodium chloride, Corros. Sci. 40 (10) (1998) 1769–1791.
[20] J.D. Hanawalt, C.E. Nelson, J.A. Peloubet, Trans. AIME 147 (1942) 273.
[21] G. Song, D. St John, The effect of zirconium grain refinement on the corrosion behaviour of magnesium-rare earth alloy MEZ, J. Light Metals 2 (2002) 1–16.